Conference on Modelling Fluid Flow (CMFF'15)
The 16th International Conference on Fluid Flow Technologies
Budapest, Hungary, September 1-4, 2015

EFFECT OF ORIENTATION OF FORCED MOTION ON THE FLOW PAST A CIRCULAR CYLINDER FOLLOWING A FIGURE-8 PATH

László BARANYI[1]

[1] Corresponding Author. Department of Fluid and Heat Engineering, University of Miskolc, 3515 Miskolc-Egyetemváros, Hungary. Tel.: +36 46 565 154, Fax: +36 46 565 471, E-mail: arambl@uni-miskolc.hu

ABSTRACT

This numerical study investigates the low-Reynolds-number flow past a circular cylinder placed in a uniform stream following a slender figure-8 path, using a thoroughly tested two-dimensional computational method based on the finite difference method. This type of two-degree-of-freedom motion have often been observed in practice. The combined effects of transverse oscillation amplitude, frequency ratio (0.9, 1.0 and 1.1), amplitude ratio (0.0, 0.1, 0.2, 0.3 and 0.4) and direction of cylinder orbit (clockwise (CW) and anticlockwise (ACW) in the upper loop of figure-8) were investigated at Reynolds number 150 on the mechanical energy transfer and the time-mean values of lift and drag. Results differ substantially depending on the direction of orientation. Mechanical energy transfer between fluid and cylinder was positive (potential danger of vortex-induced vibration) over a much larger parameter domain for ACW direction compared to CW. On the other hand, the CW case is much more prone to the occurrence of vortex switches.

Keywords: circular cylinder, drag and lift coefficients, figure-8 path, mechanical energy transfer, Reynolds number, Strouhal number

NOMENCLATURE

A_x, A_y	[-]	oscillation amplitude in x and y directions, non-dimensionalised by d
C_D	[-]	drag coefficient, $2D/(\rho U^2 d)$
C_L	[-]	lift coefficient, $2L/(\rho U^2 d)$
D	[N/m]	drag force per unit length
E	[-]	mechanical energy transfer
FR	[-]	frequency ratio, f_y/St_0
L	[N/m]	lift force per unit length
Re	[-]	Reynolds number, Ud/ν
St	[-]	Strouhal number, $f_v d/U$
T	[-]	cycle period, non-dimensionalised by d/U
U	[m/s]	free stream velocity
a_{0x}, a_{0y}	[-]	cylinder acceleration in x and y directions, non-dimensionalised by U^2/d
d	[m]	cylinder diameter, length scale
f_x, f_y	[-]	oscillation frequency in x and y directions, non-dimensionalised by U/d
f_v	[s^{-1}]	vortex shedding frequency
x,y	[-]	Cartesian co-ordinates, non-dimensionalised by d
Δt	[-]	time step, non-dimensionalised by by d/U
ν	[m^2/s]	kinematic viscosity
ρ	[kg/m^3]	fluid density
Θ	[-]	phase angle between cylinder motions in x and y directions

Subscripts and Superscripts

D	drag
fb	fixed body
L	lift
v	vortex
x, y	components in x and y directions

1. INTRODUCTION

Several engineering structures exhibit vibration problems caused by vortex shedding. Some examples of these in real life are the vibration of silos, smokestacks, underwater pipes or risers or the tube bundles of heat exchangers. When vortices are shed from the body a periodic force is generated which can cause fatigue of or damage to the structure, especially if the vortex shedding frequency is near the natural frequency of the structure and the damping is small. The noisy operation of a device can be another result of vortex-induced vibration (VIV). Due to its practical importance many researchers have dealt with one-degree-of-freedom (1-DoF) motion, most frequently cylinder oscillation transverse to the main stream

(see, e.g. [1-3]). The other type of 1-DoF motion is in-line with the main stream (see e.g. [4, 5]).

In most cases, however, vibration occurs in both transverse and in-line (streamwise) directions, leading to a two-degree-of-freedom (2-DoF) motion. Relatively few studies deal with either free or forced 2-DoF motions, two types of which have been observed in practice: (a) when the oscillation frequencies in the two directions are identical (f_x=f_y=f), resulting in an elliptical path (e.g. [6, 7]), (b) when the frequency of cylinder oscillation in the streamwise direction is approximately double that of the transverse direction (f_x=2f_y), yielding a figure-8 path (see e.g. the experimental studies [8-12]). [8, 9] have shown that when the cylinder is also free to oscillate in-line with the flow (2-DoF), the hydrodynamic forces can be very different than those observed for a cylinder oscillating only in the crossflow direction (1-DoF). The phase angle difference Θ between in-line and transverse motions of the cylinder results in not only different cylindrical paths (figure-eight, distorted figure-eight and crescent shape) but even different orientations along the path (clockwise and anticlockwise orbit on the upper loop of figure-eight), [10, 11]. It was shown in [10] that the value of Θ can alter the reduced velocity for which a transition between 2S and 2P (see [1]) shedding occurs. During the forced cylinder motion experiments in [12] the effect of phase angle Θ on lift was investigated.

In a 2-DoF free vibration numerical study [13] figure-eight and crescent shape paths were obtained, just like in the experimental studies [10, 11]. In the numerical study [14] flow around a mechanically oscillated cylinder following a figure-eight path was investigated in at Reynolds number Re=400, frequency ratios f_y/St_0=0.9, 1.0 and 1.1 and at two different A_x/A_y ratio values while varying the transverse amplitude of oscillation. They also carried out computations for both directions of orbit and found that an anticlockwise orbit in the upper loop resulted in a positive power coefficient, meaning an increased chance of VIV for a cylinder in free vibration.

The present author in [15] numerically investigated the time-mean of force coefficients and the mechanical energy transfer E between a cylinder placed in a uniform stream and forced to follow a figure-eight path and the fluid at Re=200, 250 and 300 at a fixed amplitude ratio A_x/A_y=0.14 against the frequency ratio in the lock-in domain for both clockwise (CW) and anticlockwise (ACW) directions of orbit on the upper loop of figure-eight. It was found that the flow features and the energy transfer depend strongly on the direction of orbit. For the CW orbit the value of E was negative (energy is extracted from the cylinder) in the whole parameter domain investigated, meaning that in this case there is no danger of VIV. For the ACW case, however, the opposite was obtained, indicating a potential risk of VIV in the case of an elastically supported cylinder.

The main objective of this paper is to investigate the effect of amplitude ratio (limited to slender cylinder paths in the transverse direction) and frequency ratio (ratio of cylinder oscillation frequency in transverse direction and the frequency of vortex shedding from a stationary cylinder at the same Reynolds number) on the time-mean of force coefficients, focusing on the positive mechanical energy transfer between the fluid and the cylinder.

2. COMPUTATIONAL METHOD

A non-inertial system fixed to the accelerating cylinder is used for the computation of the two-dimensional (2D), constant property, low-Reynolds number incompressible fluid flow around a circular cylinder placed in a uniform stream. The governing equations are the non-dimensional Navier-Stokes equations in a non-inertial system fixed to the moving cylinder, the equation of continuity and a Poisson equation for pressure. A no-slip boundary condition is used for the velocity and a Neumann type boundary condition for the pressure is used on the cylinder surface. At the far region potential flow is assumed.

The physical domain, which is bounded by two concentric circles with radii R_1 and R_2, is transformed into a rectangular computational domain with equidistant spacing. This mapping ensures a fine grid scale near the cylinder and a coarse grid in the far field. The transformed governing equations and boundary conditions are solved by the finite difference method. For further details see [7]. The code developed by the author has been extensively tested against experimental and computational results and good agreement was found (see [7]). In this study the dimensionless time step is 0.0005, the computational domain is characterised by R_2/R_1=160 and the grid size is 361x292.

The layout of the cylinder path is shown in Figure 1. Here U is the free stream velocity (velocity scale), d=2R_1 is the cylinder diameter (length scale), and A_x and A_y are the dimensionless amplitudes in x and y directions, respectively. Every quantity is made dimensionless by the combination of U and d. The dimensionless displacements of the forced cylinder motion x_0, y_0 in x and y directions are given by

$$x_0(t) = A_x \sin(2\pi f_x t + \Theta), \qquad (1)$$

$$y_0(t) = A_y \sin(2\pi f_y t), \qquad (2)$$

where f_x and f_y are the cylinder oscillation frequencies in x and y directions non-dimensionalised by U/d. Equations (1) and (2) ensures a figure-eight or distorted figure-eight path if f_x = 2f_y. Depending on the phase angle Θ between cylinder motions in x and y directions, clockwise (CW) or anticlockwise

(ACW) orbit can be obtained at the upper loop of figure eight:

$$f_x = 2 f_y; \quad \Theta = \pi, \quad \text{(for CW)}, \tag{3}$$

$$f_x = 2 f_y; \quad \Theta = 0, \quad \text{(for ACW)}. \tag{4}$$

Equations (3) and (4) ensure a regular figure-eight path (see Fig. 1).

The following notations are used for the amplitude ratio ε and frequency ratio FR:

$$\varepsilon = A_x / A_y, \tag{5}$$

$$\mathrm{FR} = f_y / \mathrm{St}_0. \tag{6}$$

In Eqs. (5) and (6) A_x and A_y are the dimensionless oscillation amplitudes in x and y directions, and St_0 is the dimensionless vortex shedding frequency for a stationary cylinder at that Reynolds number. The St_0 value St_0=0.18366 for Re=150 is from [16].

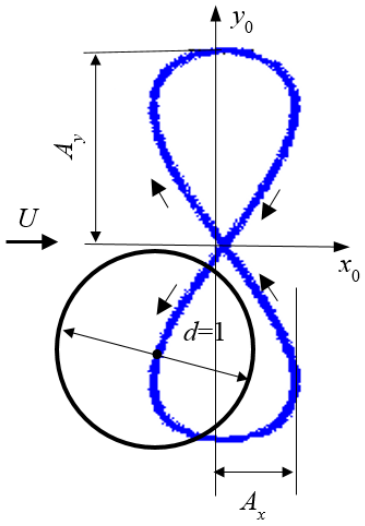

Figure 1. Layout for the figure-eight path, CW

Throughout this paper the lift (C_L) and drag (C_D) coefficients used do not contain the inertial forces originating from the non-inertial system fixed to the moving cylinder. These coefficients are often termed 'fixed body' coefficients (see [2]). The two sets of coefficients can be written as

$$C_L = C_{Lfb} + \frac{\pi}{2} a_{0y}, \; C_D = C_{Dfb} + \frac{\pi}{2} a_{0x}, \tag{7}$$

where subscript *fb* stands for fixed body (understood in an inertial system) [17]. In Eq. (7) a_{0x} and a_{0y} accelerations are the second time derivatives of cylinder displacements x_0, y_0 given in Eqs. (1) and (2). Since a_{0x} and a_{0y} are T-periodic functions their time-mean (TM) values vanishes, resulting in identical TM values for lift and drag in the two systems.

The non-dimensional mechanical energy transfer E originally introduced in [3] for a transversely oscillating cylinder is extended for a general 2-DoF motion of the cylinder in [7]:

$$E = \frac{2}{\rho U^2 d^2} \int_0^T \mathbf{F} \cdot \mathbf{v}_0 \, \mathrm{d}t = \int_0^T \left(C_D \, v_{0x} + C_L \, v_{0y} \right) \mathrm{d}t \,. \tag{8}$$

Since the frequencies in the two directions are different (see Eqs. (3) and (4)) the larger period of $T=T_y=1/f_y$ is chosen for the investigation. In Eq. (8) $\mathbf{F}$ is the force vector per unit length of cylinder, $\mathbf{v_0}=(v_{0x},v_{0y})$ are the velocity vector of the cylinder.

3. RESULTS AND DISCUSSION

During the systematic investigations the value of amplitude ratio ε is kept constant at 0, 0.1, 0.2, 0.3 and 0.4 at Re=150 and at frequency ratios of FR=0.9, 1.0 and 1.1 for both clockwise (CW) and anticlockwise (ACW) orbit on the upper lobe of figure-eight, while the transverse oscillation amplitude A_y varied. Only locked-in cases are considered in this paper. Larger ε values mean a "thicker" figure-eight path but even the largest ε value investigated ensures a relatively slender path. First the effects of flow parameters on the TM values of lift (C_L) and drag (C_D) coefficients will be shown, then effects of the mechanical energy transfer E, and finally the vicinity of a jump (due to a switch in the vortex structure) is investigated. Pre- and post-jump analysis in the vicinity of a jump was also carried out.

The FR=1.1 case, also investigated, is not shown here, as it provides little new information. At FR=1.1 there is a wider no-lock-in domain than at the lower FR values.

3.1. Effect of flow parameters on time-mean of force coefficients

The time-mean (TM) and root-mean square (rms) values of lift, drag, base pressure and torque coefficients were investigated but due to lack of space only TM of lift and drag will be shown here. The scales on the axes for each pair of figures (CW and ACW) are kept the same for ease of comparison.

Figure 2 shows the TM of lift for FR=0.9 for different amplitude ratios (ε) against the transverse oscillation amplitude A_y. The value $\varepsilon=A_x/A_y=0$ (eps=0 in the figure) means pure transverse oscillation. The top figure shows the case when the cylinder orbit on the upper loop of figure-eight is clockwise (CW) and for the bottom figure the orbit is anticlockwise (ACW). The difference for the two directions of orbit is conspicuous. For the CW case the TM of lift is zero at small A_y values. It represents 2S shedding, which means that two single vortices are shed in a vortex shedding period [1]. This is the Kármán vortex street typical for low-Re-number flow past a stationary circular cylinder placed in a uniform stream. By increasing A_y, at some critical A_y value depending on

ε, the symmetry in the flow is broken by an instability, a pitchfork bifurcation [18] starts and the TM of lift ceases to be zero any more.

This phenomenon is similar to that of the buckling rod. There are two possible solutions but only one of them are realised. There are two attractors in this non-linear system (periodic orbits in this case), each has a 'basin of attraction' in the initial condition space, and the solution is attracted to one or the other, depending on the initial conditions. By changing initial conditions a basin boundary may be crossed. As a result the solution would switch from one to the other [18]. This bifurcation starts at smaller A_y values for higher ε values: it starts at around A_y =0.3 for ε =0.4 and at around A_y =0.8 for pure transverse oscillation (ε =0). It can also be seen in the top figure that for ε =0.3 and 0.4 the solutions are first attracted to one attractor and then abruptly switch to the other, and thus jumps can be observed in the TM of lift at around A_y =0.45. For smaller ε values such switches do not occur in the parameter domain investigated.

In the bottom figure in Fig. 2 (ACW orbit) almost all TM values are zero in the investigated A_y domain. The ε =0 case shows a similar tendency to its CW counterpart but near A_y =0.8 it bifurcates to negative TM of lift values. For the thickest figure-eight path case, i.e. for ε =0.4, the TM value is zero up to around A_y =0.61, where there is a jump to a negative TM value, and remains negative as A_y increases. At this point 2S shedding ceases to exist.

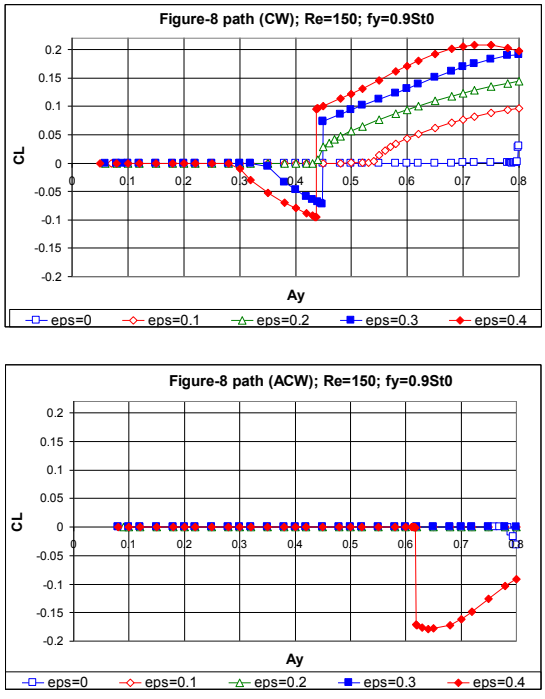

Figure 2. Time-mean value of lift against A_y at FR=0.9: top – CW; bottom – ACW

Figure 3 shows the TM of drag coefficients against A_y for FR=0.9 for different amplitude ratios ε. In the CW case, the TM of drag increases with A_y for all ε, as expected. Interestingly, TM values are lowest for the ε=0.1 and curves for ε=0 and 0.2 almost coincide. Between ε=0.2 and 0.4 the TM values increase monotonically with ε. The phenomenon that causes jumps in the TM of lift (see Fig. 2 top) has no visible effect on the TM of drag.

In the ACW orbit (Fig. 3 bottom) similar trends can be observed with some differences. One difference is that the TM values are higher for the ACW case. Another is the TM of drag is a monotonic function of amplitude ratio ε. The third is that for ε=0.4 a jump can be detected at around A_y=0.61, just like in the TM of lift curve in Fig. 2.

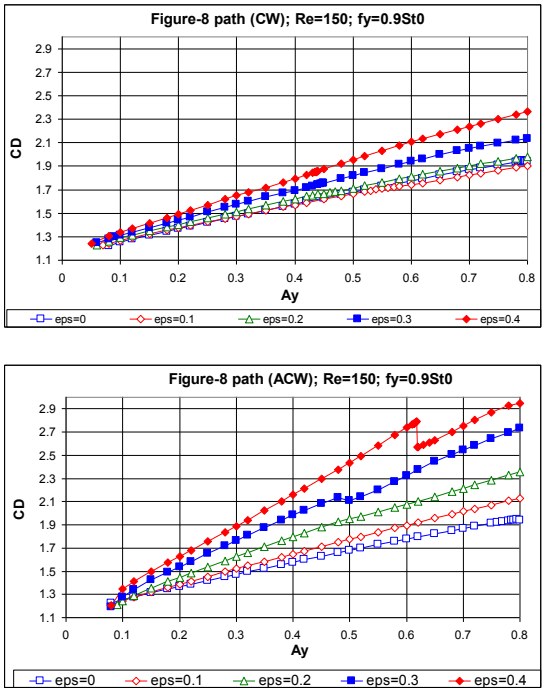

Figure 3. Time-mean value of drag against A_y at FR=0.9: top – CW; bottom – ACW

Figures 4 and 5 show the TM of lift and drag for frequency ratio FR=1.0 for both CW and ACW directions of orbit. The TM of lift for CW is shown against A_y in the top figure of Fig. 4. The similarity to the case of FR=0.9 (see Fig. 2 top) is striking. The ACW case (Fig. 4 bottom) is partly similar to its FR=0.9 counterpart (see Fig. 2 bottom) but here the TM of lift for the ε=0.3 case is not zero, there are sudden switches or jumps in both ε=0.3 and 0.4 curves and the absolute value of lift is larger than in the FR=0.9 case.

Figure 5 shows the TM of drag versus A_y. The CW case is similar to the FR=0.9 case (see Fig. 3 top) but the values are somewhat higher for the case of FR=1.0 and there are small jumps in the ε=0.3 and 0.4 curves at around A_y=0.24. As for the ACW case, comparing it to the curves for FR=0.9, one can say that the main trends are similar in the two figures, but for the ACW case for ε=0.2 there is a jump and even a

discontinuity at around A_y=0.35. As was mentioned earlier, only locked-in cases are considered in this study. Here the discontinuity means that at some A_y values the flow is not locked-in (the flow is not synchronised with the cylinder motion). For ε=0.4 two jumps are found in the curve.

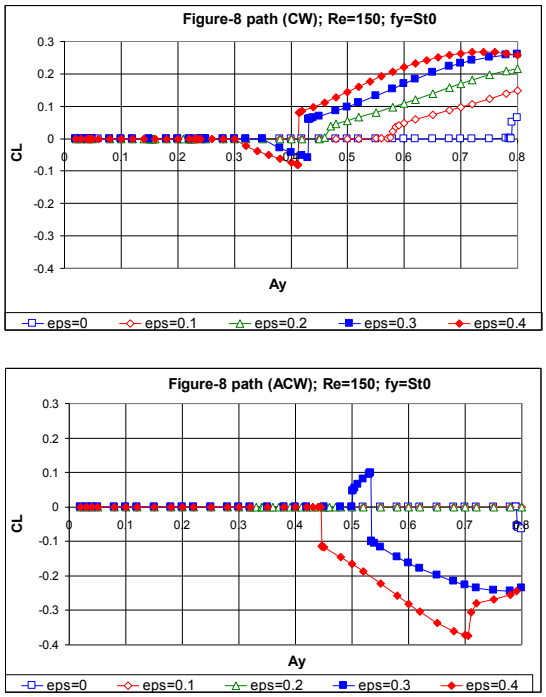

Figure 4. Time-mean value of lift against A_y at FR=1.0: top – CW; bottom – ACW

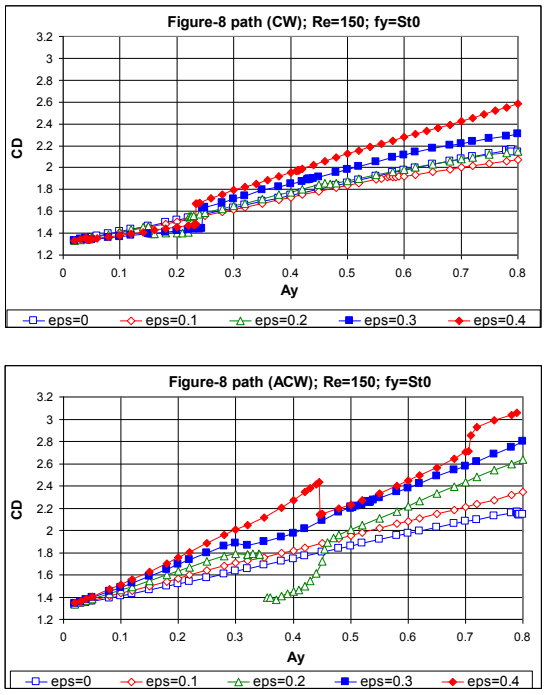

Figure 5. Time-mean value of drag against A_y at FR=1.0: top – CW; bottom – ACW

3.2. Effect of flow parameters on the mechanical energy transfer

Let us see now how the mechanical energy transfer E, defined by Eq. (8), depends on the following parameters: direction of orbit (CW or ACW), frequency ratio FR=f_y/St$_0$, amplitude ratio ε=A_x/A_y, and transverse cylinder oscillation amplitude A_y. Again, the scales on the axes for each pair of figures (CW and ACW) are kept the same for ease of comparison. Figure 6 shows E against A_y for FR=0.9 and ε=0, 0.1, 0.2, 0.3 and 0.4 for the CW orbit (top figure). It can be seen that E is decreasing with ε and that E is negative for the largest part of the parameter domain for the CW orbit. Negative E means that energy is extracted from the cylinder by the fluid. In this case the flow is acting to dampen the cylinder motion. Positive E values, however, can be dangerous for a freely vibrating (or elastically supported) cylinder because positive E amplifies the cylinder motion, since in this case the cylinder obtains energy from the flow. The bottom figure in Fig. 6 zooms in on positive E values. As can be seen, positive E values can only be found for ε=0 and 0.1. In the case of ε=0 (transverse oscillation) E is positive in the interval of 0.08 < A_y < 0.48 and the peak value in E is around 0.17, found at A_y=0.32. For ε=0.1 the value of E is even smaller (E > 0 if 0.09 < A_y < 0.28 and E_{max} is around 0.04 and at A_y=0.2). For ε=0.2, 0.3 and 0.4 no positive E values can be found in the whole investigated A_y domain for FR=0.9 and CW orbit.

Figure 7 shows E against A_y for FR=0.9 and ε=0, 0.1, 0.2, 0.3 and 0.4 for the ACW (top figure) orbit. A direct comparison of this figure with its CW counterpart (Fig. 6 top) shows that for the ACW case the absolute value of the negative E values at large A_y values is much smaller than for the CW orbit and the order of the curves belonging to different ε values is different. Hence the flow has a lower dampening effect on the vibration of an elastically supported cylinder when the orbit is ACW. The bottom figure of Fig. 7 zooms in on positive E values. As can be seen, positive E values occur for all five ε values in this case. For each curve E has a maximum and the smallest peak E values occur at ε=0, and E basically increases with increasing ε values (in contrast with the CW case; see Fig. 6 bottom). The maximum value of E is around unity, and positive E values occur for almost all of the investigated A_y domain. Comparing this figure with its CW counterpart reveals that the positive E values are much larger for the ACW case. Hence this orbit is much more dangerous in the case of a freely vibrating cylinder than the cylinder with a CW orbit.

This investigation was repeated for frequency ratio FR=1.0. The relevant computational results for E for both the CW and ACW orbits are shown in Figures 8 and 9. The CW orbit (Fig. 8 top) shows similar tendencies to its FR=0.9 counterpart (Fig. 6 top). When zooming in on the positive E values it can be seen that positive values now occur at three ε

values of 0, 0.1 and 0.2. The tendency is similar to the case of FR=0.9 (see Fig. 6 bottom) but the largest E value is about 0.4 this time. Also, jumps occur in the curve for ε=0.2.

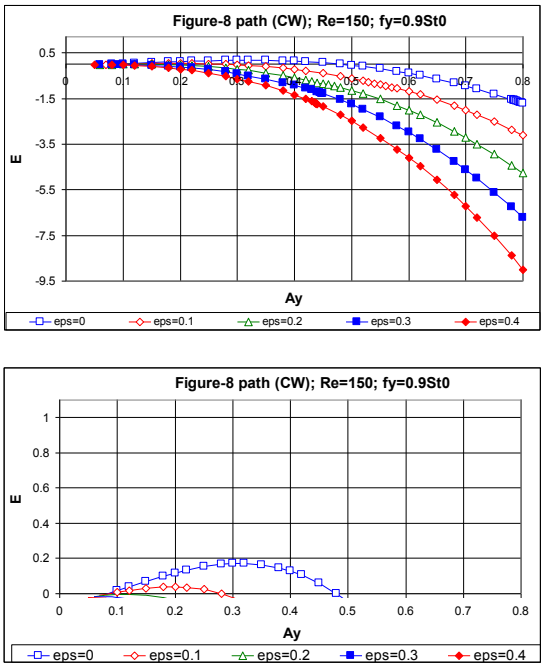

Figure 6. E against A_y at FR=0.9 and CW orbit (top); zoom in on positive E (bottom)

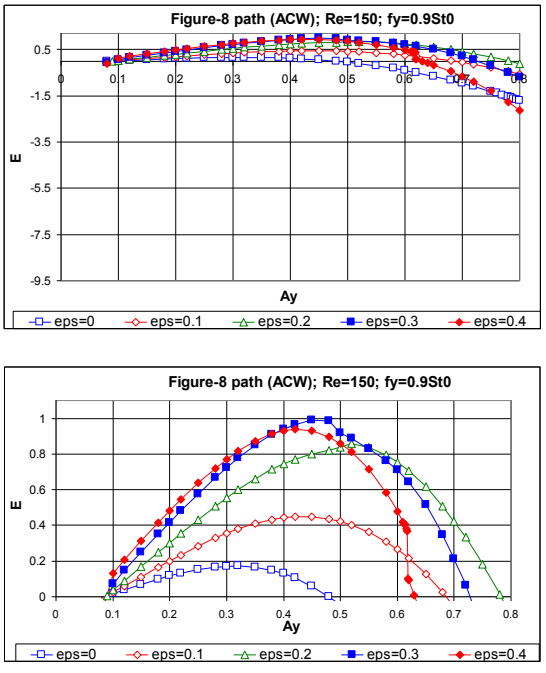

Figure 7. E against A_y at FR=0.9 and ACW orbit (top); zoom in on positive E (bottom)

Figure 9 shows the ACW case for FR=1. The top figure is very similar to its FR=0.9 counterpart (see top figures in Figs. 7 and 9). The bottom figure in Fig. 9 is also similar to the zoomed in figure for FR=0.9 for ACW orbit (see Fig. 7 bottom) with the small difference that the FR=1.0 case contains not only jumps but also non-locked in sections (see the case of ε=0.2). The peak value in E is also quite high: E=0.832 at A_y=0.4 for ε=0.4.

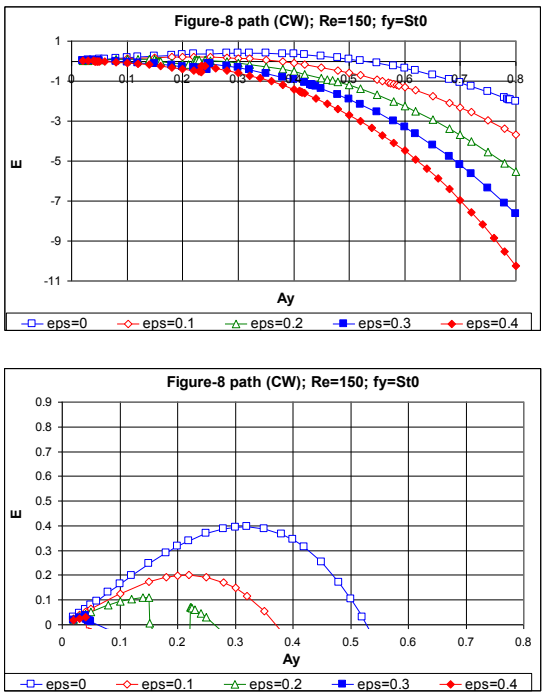

Figure 8. E against A_y at FR=1.0 and CW orbit (top); zoom in on positive E (bottom)

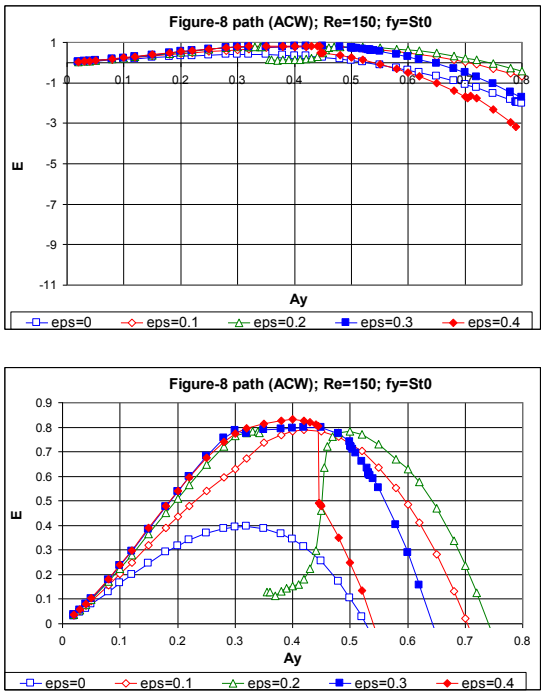

Figure 9. E against A_y at FR=1.0 and ACW orbit (top); zoom in on positive E (bottom)

3.3. Pre- and post-jump analysis

The vicinity of a jump in the TM of lift is investigated by different means, but due to lack of space only two will be shown here: a drag-lift limit cycle curve and vorticity contours before (-) and after (+) a jump. The data for the jump shown here are FR=0.9, ε=0.4, CW orbit; A_{y-}=0.4374, A_{y+}=0.4375; the jump can be seen clearly on the top figure in Fig. 2. By eliminating the time from the periodic fixed body lift and drag coefficients, the limit cycles can be obtained. The top figure in Figure 10 shows limit cycles (C_{Dfb},C_{Lfb}) for A_{y-} (thick line) and A_{y+} (thin line). Although there is just a tiny difference between oscillation amplitudes, still the limit cycle curves differ from each other quite a lot. While not obvious at first sight, these curves are mirror images to each other (flipping along the line of C_{Lfb}=0), as can also be seen in the bottom figure of Fig. 10, where the post-jump C_{Lfb} is replaced by (-C_{Lfb}). The two curves coincide with each other very well (this time both curves are plotted as thin lines).

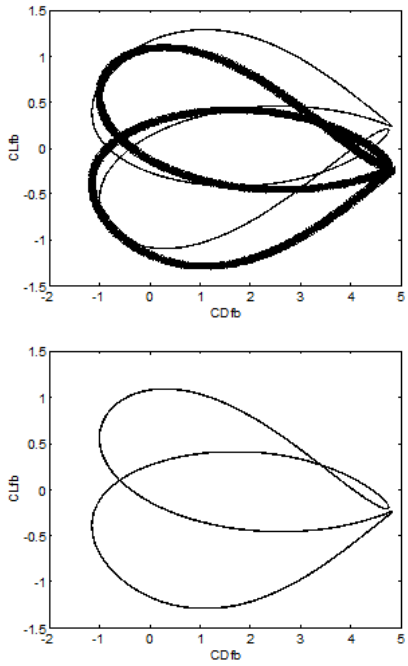

Figure 10. Limit cycle curves (FR=0.9, ε =0.4, CW), A_{y-}=0.4374 (thick line); A_{y+}=0.4375 (thin line), (C_{Dfb},C_{Lfb}) (top); (C_{Dfb},-C_{Lfb}) (bottom)

Computed vorticity contours are shown in Figure 11 for A_{y-} (top) and A_{y+} (bottom) amplitude values. The grey colour indicates negative vorticity values (rotating clockwise), and the black is positive (anticlockwise). The pre- and post-jump vorticity contours are taken at the instants of t=66T=399.2885 and t=66.5T=402.3135 (shifted by half a period), respectively. As can be seen in the two figures the vorticity contours are almost perfectly mirror images of each other, as was also found for the limit cycles. The vortex shedding mode is P+S, meaning that a pair (P) of vortices and a single (S) vortex are shed in one period [1]. Before the jump the pair of vortices are in the lower row, after the jump they switch to the upper row. The pre- and post jump time-history curves also show that they are not a mere reflection of each other; they are reflected and translated by half a period (T/2) with respect to each other. That is why the vorticity contour snapshots are also taken shifted by T/2.

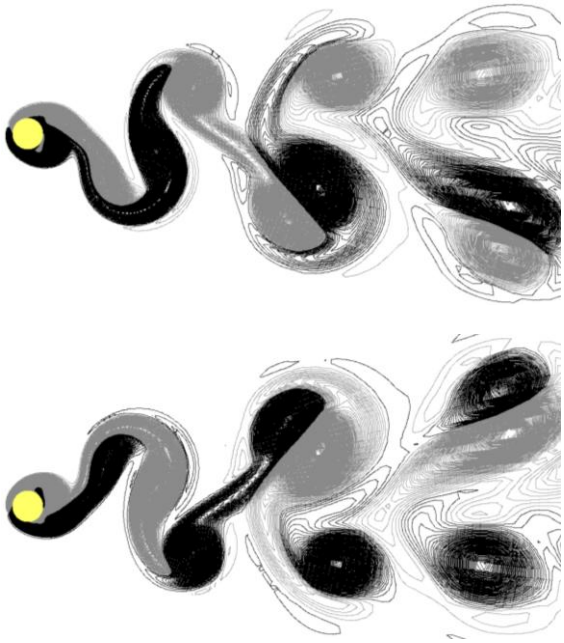

Figure 11. Vorticity contours: top pre-jump (A_{y-}=0.4374); bottom post-jump (A_{y+}=0.4375)

4. CONCLUSIONS

Flow around a circular cylinder forced to follow a slender figure-eight path is investigated numerically at frequency ratios FR=0.9, 1.0 and 1.1, Re=150, and amplitude ratios ε=A_x/A_y=0, 0.1, 0.2, 0.3 and 0.4 in the lock-in domain. Mechanical energy transfer E and time history of lift and drag are plotted against transverse oscillation amplitude A_y while other parameters are kept constant. Both clockwise (CW) and anticlockwise (ACW) orbits on the upper loop of a figure-eight path are investigated.

From the results it can be stated that

- Time-mean of lift is very sensitive to the direction of cylinder orbit;
- Energy transfer E for the CW case: E is negative in the largest part of the parameter domain, and positive E values are confined to moderate A_y values (A_y < 0.53). There are small positive E peaks for the smaller ε values (the maximum value of positive E peaks belongs to ε =0); for larger ε values there are no positive E values at all.
- Energy transfer E for the ACW case: E is positive in the largest part of the parameter domain (amplifying vibration effect). There are large positive E peaks, and the value of the

peaks increases with ε (unlike in the CW case). This situation represents a potencial risk for vortex-induced vibration VIV for free vibration cases, and can lead to fatigue of the structure.

- The pre- and post-jump analysis around a switch or jump in the value of TM of lift shows that both the drag-lift limit cycle curves and vortex contours belonging to pre- and post-jump amplitude values are mirror images of each other.

Future investigations could include computations at further Reynolds numbers or frequency ratios.

ACKNOWLEDGEMENTS

The work was carried out as part of the TÁMOP-4.2.1.B-10/2/KONV-2010-0001 project in the framework of the New Hungarian Development Plan. The realization of this project is supported by the European Union, co-financed by the European Social Fund. The author would like to thank Mr. L. Daróczy for designing the flow visualization software used in Fig. 11.

REFERENCES

[1] Williamson, C.H.K., 1988, "Vortex formation in the wake of an oscillating cylinder", *Journal of Fluids and Structures*, Vol. 2, pp. 355–381.

[2] Lu, X.Y., and Dalton, C., 1996, "Calculation of the timing of vortex formation from an oscillating cylinder", *Journal of Fluids and Structures*, Vol. 10, pp. 527–541.

[3] Blackburn, H.M., and Henderson, R.D., 1999, "A study of two-dimensional flow past an oscillating cylinder", *Journal of Fluid Mechanics*, Vol. 385, pp. 255–286.

[4] Wootton, L.R., 1972, *Resume on Full-scale Tests on Oscillation of Piles in Marine Structures*, Construction Industry Research & Information Association (CIRIA), London

[5] Al-Mdallal, Q.M., Lawrence, K.P., and Kocabiyik, S., 2007, "Forced streamwise oscillations of a circular cylinder: Locked-on modes and resulting fluid forces", *Journal of Fluids and Structures*, Vol. 23, pp. 681–701.

[6] Didier, E., and Borges, A.R.J., 2007, "Numerical predictions of low Reynolds number flow over an oscillating circular cylinder", *Journal of Computational and Applied Mechanics*, Vol. 8(1), pp. 39–55.

[7] Baranyi, L., 2008, "Numerical simulation of flow around an orbiting cylinder at different ellipticity values", *Journal of Fluids and Structures*, Vol. 24, pp. 883–906.

[8] Jauvtis, N., and Williamson, C.H.K., 2004, "The effect of two degrees of freedom on vortex-induced vibration and at low mass and damping", *Journal of Fluid Mechanics*, Vol. 509, pp. 23–62.

[9] Dahl, J.M., Hover, F.S., and Triantafyllou, M.S., 2006, "Two-degree-of-freedom vortex-induced vibrations using a force assisted apparatus", *Journal of Fluids and Structures*, Vol. 22, pp. 807–818.

[10] Jeon, D., and Gharib, M., 2001, "On circular cylinders undergoing two-degree-of-freedom forced motions", *Journal of Fluids and Structures*, Vol. 15, pp. 533–541.

[11] Sanchis, A., Sælevik, G., and Grue, J., 2008, "Two-degree-of-freedom vortex-induced vibrations of a spring-mounted rigid cylinder with low mass ratio", *Journal of Fluids and Structures*, Vol. 24, pp. 907–919.

[12] Dahl, J.M., Hover, F.S., and Triantafyllou, M.S., 2008, "Third harmonic lift forces from phase variation in forced crossflow and in-line cylinder motions", Proc. *9th International Conference on Flow-Induced Vibrations*, Prague, pp. 799–804.

[13] Prasanth, T.K., and Mittal, S., 2009, "Flow-induced oscillation of two circular cylinders in tandem arrangement at low Re", *Journal of Fluids and Structures*, Vol. 25, pp. 1029–1048.

[14] Peppa, S., Kaiktsis, L., and Triantafyllou, G.S., 2010, "The effect of in-line oscillation on the forces of a cylinder vibrating in a steady flow", *American Society of Mechanical Engineers, Fluids Engineering Division (Publication) FEDSM*, 3 (PARTS A and B), pp. 21–28.

[15] Baranyi, L., 2012, "Simulation of a low-Reynolds number flow around a cylinder following a figure-8-path", *International Review of Applied Sciences and Engineering*, Vol. 3(2), pp. 133–146.

[16] Posdziech, O., and Grundmann, R., 2007, "A systematic approach to the numerical calculation of fundamental quantities of the two-dimensional flow over a circular cylinder", *Journal of Fluids and Structures*, Vol. 23, pp. 479–499.

[17] Baranyi, L., 2005, "Lift and drag evaluation in translating and rotating non-inertial systems", *Journal of Fluids and Structures*, Vol. 20(1), pp. 25–34.

[18] Strogatz, S.H., 1994, *Nonlinear Dynamics and Chaos*. Westview Press, Cambridge MA.